

Received ; Accepted

The galaxy density environment of gamma-ray burst host galaxies^{1,2}

Carlos G. Bornancini, Héctor J. Martínez³, Diego G. Lambas³

*Grupo de Investigaciones en Astronomía Teórica y Experimental, IATE
Observatorio Astronómico, Universidad Nacional de Córdoba
Laprida 854, X5000BGR, Córdoba, Argentina*

bornancini@oac.uncor.edu, julian@oac.uncor.edu, dgl@oac.uncor.edu

Emeric Le Floc'h

*Steward Observatory, University of Arizona
933 Cherry Av., Tucson, AZ, 85721, USA*

elefloch@as.arizona.edu

I. Félix Mirabel⁴

*CEA/DSM/DAPNIA Service d'Astrophysique
F-91191 Gif-sur-Yvette, France*

mirabel@discovery.saclay.cea.fr

and

Dante Minniti

*Department of Astronomy, Pontificia Universidad Católica
Vicuña Mackenna 4860, Casilla 306 Santiago 22, Chile*

dante@astro.puc.cl

¹Based on observations with the Very Large Telescope, obtained at the European Southern Observatory in Chile under Proposal 67.B-0611(A)

²Based on observations made with the NASA/ESA *Hubble Space Telescope (HST)*, obtained at the Space Telescope Science Institute, which is operated by the Association of Universities for Research in Astronomy, Inc. under NASA contract NAS5-2655

³ Consejo Nacional de Investigaciones Científicas y Técnicas (CONICET), Avenida Rivadavia 1917, C1033AAJ, Buenos Aires, Argentina.

⁴Instituto de Astronomía y Física del Espacio, cc67, suc28. 1428 Buenos Aires, Argentina.

ABSTRACT

We analyze cross-correlation functions between Gamma-Ray Burst (GRB) hosts and surrounding galaxies. We have used data obtained with the Very Large Telescope at Cerro Paranal (Chile), as well as public Hubble Space Telescope data. Our results indicate that Gamma-Ray Burst host galaxies do not reside in high galaxy density environments. Moreover, the host-galaxy cross-correlations show a relatively low amplitude. Our results are in agreement with the cross-correlation function between star-forming galaxies and surrounding objects in the HDF-N.

Subject headings: gamma rays: bursts — cosmology: general

1. Introduction

The origin of cosmological Gamma-Ray Bursts (GRBs) is still one of the outstanding problems in modern astronomy (van Paradijs et al. 1997). Over the past half decade, the discovery of localized transients in the small error boxes of GRBs has led to intense multi-wavelength campaigns and many advances have been made in understanding the nature of the bursts and their afterglows throughout the electromagnetic spectrum (see for instance van Paradijs, Kouveliotou, & Wijers (2000)).

The scenario for the origin of GRBs include either the merging of two collapsed objects such as black holes or neutron stars merge (Narayan, Paczynski, & Piran 1992) or the cataclysmic destruction of massive stars (supernovae or hypernovae) (Woosley 1993; MacFadyen & Woosley 1999). In the first scenario, GRBs can occur long after the star formation episodes in the nucleus since the merging characteristic time scale is as long as $\gtrsim 1$ Gyr. In the second scenario the host galaxies are likely to be on-going significant star formation.

Bloom, Kulkarni, & Djorgovski (2002) analyzed the observed offset distribution of Gamma-Ray Burst from their host galaxies, and found a strong connection of GRB localization with the UV light of their host galaxies. This provides a significant observational evidence for the correlations between GRBs and star-forming regions.

The characteristics of the physical environment surrounding the bursts may provide strong constraints for the origin of these events. As suggested by MacFadyen & Woosley (1999) in the collapsar model, GRBs could be produced by rotating massive stars in which the accretion of a helium core leads to the prompt formation of a black hole. Low metallicity in the stellar envelope reduces the mass loss and inhibits the loss of angular momentum by

the star. Star formation in regions of low metallicity are likely to generate GRBs so that dwarf and sub-luminous galaxies would be preferred host of these events (see for instance Le Floc'h et al. (2003)).

This model is supported by the $\text{Ly}\alpha$ emission from GRB host galaxies which show a preference to be metal poor and with on-going star formation in a dust poor environment (Fynbo et al. 2002, 2003).

Analyzing the properties of the host galaxies of GRBs, Le Floc'h et al. (2003) found that GRB host galaxies are sub-luminous in the K -band and exhibit very blue colors, not comparable to the luminous star-burst and/or reddened sources observed at high redshifts in the infrared and sub-millimeter deep surveys.

There is new evidence that at least some Gamma-Ray Bursts are related to supernovae: the association of GRB 980425 with the peculiar Type Ic SN 1998bw (Galama et al. 1998), and also the recent spectroscopic discovery of the SN 2003dh associated with GRB 030329 (Hjorth et al. 2003; Stanek et al. 2003). These observations provide a very solid confirmation of the association of some GRBs with the death of massive stars in strong star formation regions.

At the present it is unknown if GRB host galaxies are preferentially located in dense environments, or if there is any correlation between the local density of galaxies and the presence of a GRB. So far, there are only two works on the environment of GRB host galaxies. Fynbo et al. (2002) studying the $\text{Ly}\alpha$ emission of two GRB fields (GRB 000301C & GRB 000926), found a number of galaxies at the same redshift of GRB hosts without signs of overdensity at small scales. Moreover, the lack of blank fields at a similar depth prevented these authors to conclude if GRB hosts reside in overdense regions. From an analysis of photometric redshifts of galaxies in the field of GRB 000210, Gorosabel et al. (2003) found that there is no obvious concentration of galaxies around the host. Another case, the afterglow of GRB 980613 was located close to a very compact object inside a complex region consisting of star-forming knots and/or interacting galaxy fragments (Hjorth et al. 2002; Djorgovski, Bloom, & Kulkarni 2003). If these host galaxies are associated with the underlying large scale structure of the universe, then they should show similar galaxy clustering properties of normal galaxies.

In this paper we examine the nature of the density enhancement of galaxies around GRB host galaxies by studying the cross-correlation function between GRB hosts and the surrounding galaxy distribution.

This paper is organized as follows: Section 2 describes the sample of GRB host galaxies analyzed, the source extraction and photometry techniques. We analyze galaxy source counts

in Section 3. Section 4 deals with the angular-cross correlation analysis of galaxies around GRB host galaxies. Finally we discuss our results in Section 5.

2. Data

The near-IR data were obtained with the Infrared Spectrometer And Array Camera (ISAAC) on the Very Large Telescope (VLT) at Paranal, (Chile) between March 2000 and September 2001 under photometric conditions. A K_s filter (2.0-2.3 μm) was used. The focal lens configurations resulted in a respective pixel size of $0''.148$. All the images were obtained under optimum seeing conditions with FWHM in the range $0''.6$ and $1''.5$. For the ISAAC observations, we reached a total on-source integration time of 1 hour per object. A full description of sample selection, observations and image reductions is given in Le Floc'h et al. (2003). Our sample sources is listed in Table 1, together with the position, spectroscopic redshift determinations taken from the literature, the K_s -band magnitudes of the host galaxies and the 1.5σ limiting magnitude per field.

The optical GRBs sample used in this work consist in 19 *HST*/STIS GRB host galaxies images. These observations were taken from Hubble Space Telescope (*HST*) STIS imaging data from the Cycle 9 program GO-8640 “A Survey of the Host Galaxies of Gamma-Ray Bursts” ((Holland et al. 2000a) ¹). Images were obtained with the 50CCD filter (clear, pivot $\lambda_o=5835$ Å, hereafter CL) and F28X50LP (long pass, pivot $\lambda_o=7208$ Å, hereafter LP). The data was pre-processed using the standard STIS pipeline and combined using the DITHER (v2.0) software (Fruchter & Hook 2002) as implemented in IRAF² (v2.11.3) and STSDAS (v2.3). The STIS images were drizzled using ‘pixfrac=0.6’ and ‘scale=0.5’ (giving a final pixel size of $0''.0254$). Images were selected for having an optical and/or radio bright afterglow with the deepest observations available in the 50CCD images. For the STIS zero-points, we adopted the values found by Gardner et al. (2000) for the HDF–South in the AB system (Oke 1971). The zero-points used were therefore $ZP_{CL} = 26.387$ and $ZP_{LP} = 25.291$. We have measured a PSF from the STIS images with a FWHM= 0.083 – 0.085, similar to that obtained by Gardner et al. (2000) in the HDF–S STIS analysis. We adopt this value for images without stars present in the field. *HST*/STIS sources are listed in Table 2, for the 50CCD filter, together with the position, spectroscopic redshift determinations taken from the literature, the CL band magnitudes of the host galaxies, the total on-source exposure time

¹Data and further information available at http://www.ifa.au.dk/~hst/grb_hosts/index.html

²Image Reduction and Analysis Facility (IRAF), a software system distributed by the National Optical Astronomy Observatories (NOAO).

and the 2σ limiting magnitude per field.

2.1. Source extraction and photometry

For object detection and photometry we used the SExtractor software package version 2.1 (Bertin & Arnouts 1996). For the ISAAC images, the source extraction parameters were set such that, to be detected, an object must have a flux in excess of 1.5 times the local background noise level over at least N connected pixels, where N was varied according to the seeing conditions (about ~ 10 – 15 connected pixels).

SExtractor’s `MAG_BEST` estimator was used to determine the magnitudes of the sources; this yields an estimate for the total magnitude using first Kron’s (1980) moment algorithm.

In this work we choose all objects (galaxies) with stellaricity index < 0.8 , for the ISAAC images. The result of the detection process was inspected visually in order to ensure that no obvious objects were missed, and that no false detections were entered into the catalogs. Saturated objects and objects lying in the image boundaries were rejected from the catalogs. The final effective field of view is $2'2 \times 2'2$, after spurious detections near boundary regions are rejected.

For the *HST*/STIS images, after extensive tests with SExtractor using different input parameters, it became clear that no single set of parameters could satisfy to create a catalog that would reach the faintest depth for isolated objects and faint companions of bright galaxies. This is a standard problem with SExtractor and at the moment an ideal solution does not exist. For example, Casertano et al. (2000) and Gardner et al. (2000) ran SExtractor two times with different detection thresholds. In this way, however, it is not easy to achieve consistent estimates of the fluxes with different thresholds. For these reasons, we have used a detection threshold corresponding to an isophote of 2σ and objects were required a minimum area of 10 connected pixels above this threshold and a stellaricity index `CLASS_STAR` < 0.95 , for an object to be a galaxy. After this, spurious objects in correspondence with stellar diffraction spikes and spurious galaxies detected from the spiral arm fragmentation of nearby galaxies were removed from the final catalog. The final effective field of view for the STIS images is $25''.6 \times 25''.6$.

3. Near-IR and Optical Galaxy Number Counts

In order to check for completeness in the sample analyzed, we have computed the mean number of galaxies per unit area for the fields. The results are plotted in Figure 1. Error bars were estimated using Poisson counting statistics on the raw galaxy counts. In Figure 1 (right panel), we compare our determinations with the K_s number counts in the Chandra Deep Field (CDF) and in the Hubble Deep Field South (HDF–S) (Saracco et al. 2001) and with determinations from the NTT Deep Field (Saracco et al. 1999). We also compare our counts to those of other K -band surveys from Moustakas et al. (1997), McLeod et al. (1995), Djorgovski et al. (1995), as well as from the Subaru Deep Field (Totani et al. 2001). Our K_s number counts derived here are systematically lower than those from the literature, in the range $20 < K < 22$, which could be an indication of lack of many faint galaxies in these GRBs fields. We have also computed the differential galaxy counts in the 50CCD (CL) images, (see Figure 1, left panel). Error bars were estimated using Poissonian errors. We compare our determinations with the 50CCD number counts from HDF-S STIS imaging (Gardner et al. 2000). For comparison, we plot the WFPC2 HDF-N galaxy counts in $F606W$ from Williams et al. (1996) from Volonteri, Saracco, Chincarini, & Bolzonella (2000), from the HDF–S and HDF–N and in $F450W$ from Metcalfe et al. (2001). These results are fully consistent with those in the literature.

4. Angular cross-correlation analysis

In this section we analyze the clustering of galaxies around GRB host galaxies. We compute the angular two point cross-correlation function $\omega(\theta)$ between the GRB host galaxies and the galaxies in their fields for the ISAAC near-IR images and for the *HST*/STIS images (tracer galaxies). We have used the following estimator of the angular cross-correlation function, (Peebles 1980):

$$\omega(\theta) = \frac{n_R}{n_G} \frac{DD(\theta)}{DR(\theta)} - 1 \quad (1)$$

where n_G and n_R are the numbers of galaxies in the sample and in a random sample respectively, $DD(\theta)$ is the number of real pairs host-galaxy separated by an angular distance in the range $\theta, \theta + \delta\theta$, and $DR(\theta)$ are the corresponding pairs when considering the random galaxy sample. We have also computed the auto-correlation function of the tracer galaxies in all fields analyzed which serves to compare the relative clustering strength around GRB hosts, and around typical galaxies.

We estimate correlation function error bars using the field-to-field variation:

$$\sigma^2 = \frac{1}{N-1} \sum_{i=1}^N \frac{DR_i(\theta)}{DR(\theta)} [\omega_i(\theta) - \omega(\theta)]^2 \quad (2)$$

where the subscript i stands for each individual frame. The field-to-field errors are 1σ standard deviations of the correlation function between fields, and are inverse variance-weighted to account for the different numbers of sources on each field. Myers et al. (2003) conclude that these variations provide suitable estimates of correlation uncertainties accounting for cosmic variance and differences of image photometric zero-point calibrations.

The finite area of the images implies a systematic amplitude offset known as the integral constraint C , such that $\omega_{obs}(\theta) = A(\theta^{1-\gamma} - C)$. The integral constraint can be computed numerically using a random-random sample:

$$C = \frac{\sum RR(\theta)\theta^{1-\gamma}}{\sum RR(\theta)}, \quad (3)$$

where $RR(\theta)$ is the number of random pairs of objects with angular distances between θ and $\theta + \delta\theta$. For our sample geometry, and assuming $\gamma = 1.8$, we find $C = 0.062 \text{ arcsec}^{-0.8}$, for ISAAC images and $C = 0.13 \text{ arcsec}^{-0.8}$ for *HST*/STIS images.

In Figure 2 and 3 we show the resulting host-galaxy two-point cross-correlation functions for three samples of tracer galaxies: $K_s < 21.5$, $K_s < 19$, and $19.5 < K_s < 21.5$ in the ISAAC images. These magnitudes limits are consistently with the K -band photometry and spectroscopic redshifts determinations of field galaxies (see Figure 2 in Le Floch et al. (2003)). In the same figures we have computed the auto-correlations functions of the tracer galaxies in the same magnitudes range. The amplitude of the auto-cross correlation function is $A = (0.8 \pm 0.3) \text{ arcsec}^{0.8}$, for the all tracer galaxies sample with $K_s < 21.5$; and $A = (0.56 \pm 0.33) \text{ arcsec}^{0.8}$ for tracers galaxies with $19.5 < K_s < 21.5$.

We have also performed this computation for the *HST*/STIS images which are shown in Figure 4. In this figure we can appreciate the host-galaxy cross-correlation function in the 50CCD images for tracer galaxies with $CL < 28$ around all host galaxies quoted in Table 2 (filled triangles).

We have also explored different intervals of magnitudes and the effect on the results of excluding hosts that are either too distant ($z > 2$), or relatively close ($z < 0.7$) in order to avoid very faint galaxy images and large angular scales. In Figure 4 we show the resulting

host-galaxy cross-correlation functions for tracer galaxies with $\text{CL} < 28$ around host galaxies with spectroscopic redshift determinations in the range $0.7 < z < 2$ (Filled circles). The amplitude of the auto-cross correlation function is $A = (0.5 \pm 0.2) \text{ arcsec}^{0.8}$, for the all tracer galaxies sample with $\text{CL} < 28$; and $A = (0.30 \pm 0.17) \text{ arcsec}^{0.8}$ for tracers galaxies around GRB host galaxies with spectroscopic redshifts in the range $0.7 < z < 2$ in the same magnitude range.

In this figure we have not included GRB 990705, because this GRB host is located behind the outskirts of the Large Magellanic Cloud (LCM) and it is expected a stronger contamination in the SExtractor point source identification.

We can see here that there is not a significant GRB host-galaxy cross-correlation amplitude. In similar analyzes, (Best 2000; Bornancini et al. 2004), found that radio galaxies and Ultra Steep Spectrum radio sources with comparable redshifts than our GRB sample ($z \simeq 1$). show significant cross-correlations with neighboring galaxies (shown as dotted and dashed lines in Figure 2, right panel) indicating that these sources are likely to reside in proto-cluster environments. By contrast, the lack of a cross-correlation signal in our GRB fields provides clear evidence that the neighborhood of GRB hosts is of significant lower galaxy overdensity than groups and clusters. This is reinforced by the fact that GRB-galaxy cross-correlations have a lower amplitude than the galaxy auto-correlation function in these fields for the two limiting magnitudes analyzed.

We have restricted to tracer galaxies beyond an angular radius $\theta_p > 2''.0$ from the host. We adopt this value to avoid the numerous knots or galaxy fragments, observed in some host complex systems and the surrounding galaxies. It can be appreciated in these figures a significant anti-correlation signal between GRB hosts and surrounding galaxies, indicating that GRB hosts reside in regions strongly biased to low local galaxy densities.

We have also tested for possible bias in the detection of objects near the edges of the frames of GRBs images. We have computed auto-correlation analysis for objects with $\text{CLASS_STAR} > 0.8$ for the ISSAC images and those with $\text{CLASS_STAR} > 0.95$ for the *HST*/STIS images, identified in our images as point sources (stars). We find that stars are uncorrelated on the sky, as shown in Figure 5 for $K_s < 20$. We find similar values for $\text{CL} < 28$ and $\text{CL} < 26$ in the *HST*/STIS images. The lack of signal for these samples indicates the absence of significant systematic effects in our analysis.

In order to compare these results with galaxy samples with well determined characteristics, we have computed the angular cross-correlation analysis between star-forming galaxies,

early-type galaxies, infrared galaxies (ISO sources), and tracer galaxies in the Hubble Deep Field North.

For this purpose, we have considered blue spiral and irregular galaxies from Rodighiero et al. (2000, 2001) with $H - K < 0.7$. The sample of ellipticals was selected from Stanford et al. (2003). The infrared selected galaxies was selected from ISOCAM observations in the Hubble Deep Field (Aussel, Cesarsky, Elbaz, & Starck 1999). All sources were selected in the redshift range of $0.5 < z < 1.2$. HDF tracer galaxies correspond to Fernández-Soto, Lanzetta, & Yahil (1999), extracted in the F606W filter. The results are plotted in Figure 6, for tracer galaxies with $F606W < 27$. We estimate correlation function error bars using uncertainties derived from the Bootstrap re-sampling techniques. We find a low cross-correlation amplitude at small angular scales, similar to those obtained in our *HST*/STIS images, in comparison to bright early-types galaxies and ISO sources in the same redshift range (see Figure 6).

5. Discussion and conclusions

We have analyzed different data sets corresponding to deep imaging in the field of Gamma-Ray Burst hosts. A remarkable low correlation amplitude at small angular scales is detected from the cross-correlation of GRB’s and the surrounding galaxies in all samples analyzed. The reliability of the results presented in this work can be judged from the lack of correlation of stars in *ISAAC* and *HST*/STIS images. By contrast, the galaxy-galaxy correlation function obeys the usual power-law shape with a significant signal at small separations. Given that these correlation functions were computed using angular positions, any effect in real space would be diluted by projection of foreground and background objects.

A comparison with a similar data set, centered in USS sources, indicates the very different environment of these two types of objects. While USS sources clearly reside in rich environments, GRBs are likely to reside in a typical or even lower galaxy density environment. Moreover the amplitude of the autocorrelation function of galaxies is larger than that of the GRB-galaxy cross-correlation.

In the *HST*/STIS fields GRB-tracers cross-correlation functions are significantly lower than early-type-tracers cross correlations. In addition, GRB targets have a lower cross correlation amplitude than ISO and early-type galaxy targets. This suggests that the star formation events associated to GRBs occur in particularly low density environments, a result that is supported by the fact that objects formed in global underdense regions are expected to be biased to low luminosity, consistent with GRB hosts characteristics (Le Floch et al.

2003).

This work was partially supported by the Consejo Nacional de Investigaciones Científicas y Técnicas, Agencia de Promoción de Ciencia y Tecnología, Fundación Antorchas and Secretaría de Ciencia y Técnica de la Universidad Nacional de Córdoba. We acknowledge support from the SETCIP/CONICYT joint grant CH-PA/01-U01. Dante Minniti is supported by FONDAF Center for Astrophysics 15010003.

REFERENCES

- Aussel, H., Cesarsky, C. J., Elbaz, D., & Starck, J. L. 1999, A&A, 342, 313
- Bertin E., Arnouts S., 1996, A & A Supp. 117, 393.
- Best, P. N. 2000, MNRAS, 317, 720
- Bloom, J. S., Frail, D. A., Kulkarni, S. R., et al. 1998, ApJ, 508, L2
- Bloom, J. S. et al. 1999, Nature, 401, 453
- Bloom, J. S., Djorgovski, S. G. & Kulkarni, S. R. 2002, ApJ, 554, 678
- Bloom, J. S., Kulkarni, S. R., & Djorgovski, S. G. 2002, AJ, 123, 1111
- Bloom, J. S., Berger, E., Kulkarni, S. R., Djorgovski, S. G., & Frail, D. A. 2003, AJ, 125, 999
- Bornancini, C. G., Martínez, H. J., Lambas, D. G., de Vries, W., van Breugel, W., De Breuck, C. & Minniti, D., 2004, AJ in press (astro-ph/0310264)
- Casertano, S. et al. 2000, AJ, 120, 2747
- Castro-Tirado, A. J., Sokolov, V. V., Gorosabel, J., et al. 2001, A&A, 370, 398
- Djorgovski, S. et al. 1995, ApJ, 438, L13
- Djorgovski, S. G., Bloom, J. S., & Kulkarni, S. R. 2003, ApJ, 591, L13
- Djorgovski, S. G., Kulkarni, S. R., Bloom, J. S., Goodrich, R., Frail, D. A., Piro, L., & Palazzi, E. 1998, ApJ, 508, L17
- Fernández-Soto, A., Lanzetta, K. M., & Yahil, A. 1999, ApJ, 513, 34
- Fruchter, A. & Pian, E. 1998, GRB Circular Network, 151, 1
- Fruchter, A. S., Thorsett, S. E., Metzger, M. R., et al. 1999, ApJ, 519, L13
- Fruchter, A. S. et al. 1999, ApJ, 516, 683
- Fruchter, A., Vreeswijk, P., Sokolov, V., & Castro-Tirado, A. 2000, GRB Circular Network, 872, 1
- Fruchter, A., Hook, R., & Pian, E. 2000, GRB Circular Network, 757, 1

- Fruchter, A., Sahu, K., Gibbons, R., Petro, L., & Ferguson, H. 2000, GRB Circular Network, 565, 1
- Fruchter, A., Vreeswijk, P., & Nugent, P. 2001, GRB Circular Network, 1029, 1
- Fruchter, A. & Vreeswijk, P. 2001, GRB Circular Network, 1063, 1
- Fruchter, A. & Metzger, M. 2001, GRB Circular Network, 1061, 1
- Fruchter, A. S. & Hook, R. N. 2002, Publ. Astron. Soc. Pac., 114, 14
- Fynbo, J. P. U. et al. 2002, A&A, 388, 425
- Fynbo, J. P. U. et al. 2003, A&A, 406, L63
- Galama, T. J. et al. 1998, Nature, 395, 670
- Gardner, J. P. et al. 2000, AJ, 119, 486
- Gorosabel, J. et al. 2003, A&A, 400, 127
- Hjorth, J. 2000, GRB Circular Network, 731, 1
- Hjorth, J. et al. 1999, GRB Circular Network, 219, 1
- Hjorth, J., Thomsen, B., Nielsen, S. R., et al. 2002, ApJ, 576, 11
- Hjorth, J. et al. 2003, Nature, 423, 847
- Holland, S. 2000a, GRB Circular Network, 778, 1
- Holland, S. 2000b, GRB Circular Network, 777, 1
- Holland, S. 2000c, GRB Circular Network, 749, 1
- Holland, S. 2000d, GRB Circular Network, 726, 1
- Holland, S. et al. 2000a, GRB Circular Network, 698, 1
- Holland, S., Andersen, M., Hjorth, J., et al. 2000b, GCN 753
- Holland, S. et al. 2001, A&A, 371, 52
- Jaunsen, A. O. et al. 2001, ApJ, 546, 127
- Jaunsen, A. O. et al. 2003, A&A, 402, 125

- Jensen, B. L., Fynbo, J. U., Gorosabel, J., et al. 2001, *A&A*, 370, 909
- Kulkarni, S. R. et al. 1998, *Nature*, 393, 35
- Kron, R. G., 1980, *ApJS*, 43, 305
- Lamb, D. Q., Castander, F. J., & Reichart, D. E. 1999, *A&AS*, 138, 479
- Le Floc’h E., Duc P. A., Mirabel I.F., Sanders D.B., Bosch G., Rodrigues I., Courvoisier T. J. L., Mereghetti S., Melnick J., 2002.
- Le Floc’h, E. et al. 2003, *A&A*, 400, 499
- MacFadyen, A. I. & Woosley, S. E. 1999, *ApJ*, 524, 262
- McLeod, B. A., Bernstein, G. M., Rieke, M. J., Tollestrup, E. V., & Fazio, G. G. 1995, *ApJS*, 96, 117
- Metcalfe, N., Shanks, T., Campos, A., McCracken, H. J., & Fong, R. 2001, *MNRAS*, 323, 795
- Moustakas, L. A., Davis, M., Graham, J. R., Silk, J., Peterson, B. A., & Yoshii, Y. 1997, *ApJ*, 475, 445
- Myers, A. D., Outram, P. J., Shanks, T., Boyle, B. J., Croom, S. M., Loaring, N. S., Miller, L., & Smith, R. J. 2003, *MNRAS*, 342, 467
- Narayan, R., Paczynski, B., & Piran, T. 1992, *ApJ*, 395, L83
- Odewahn, S. C. et al. 1998, *ApJ*, 509, L5
- Oke, J. B. 1971, *ApJ*, 170, 193
- Peebles, P. J. E., 1980, “The Large-Scale Structure of the Universe”, Princeton University Press.
- Piro, L., Frail, D. A., Gorosabel, J., et al. 2002, *ApJ*, 577, 68
- Rodighiero, G., Granato, G. L., Franceschini, A., Fasano, G., & Silva, L. 2001, *VizieR Online Data Catalog*, 336, 40517
- Rodighiero, G., Granato, G. L., Franceschini, A., Fasano, G., & Silva, L. 2000, *A&A*, 364, 517

- Saracco P., Giallongo S., Cristiani S., D’Odorico S., Fontana A., Iovino A., Poli F., Vanzella E., 2001 A&A, 371, 1
- Saracco P., D’Odorico S., Morwood A., Buzzoni a., Culy J. G., Lidman C., 1999, *Å*, 349, 751
- Schaefer, B. E. et al. 1999, ApJ, 524, L103
- Stanek, K. Z. et al. 2003, ApJ, 591, L17
- Stanford, S. A. et al. 2003, preprint (astro-ph/0310231)
- Totani, T., Yoshii, Y., Maihara, T., Iwamuro, F., & Motohara, K. 2001, ApJ, 559, 592
- van Paradijs, J. et al. 1997, Nature, 386, 686
- van Paradijs, J., Kouveliotou, C., & Wijers, R. A. M. J. 2000, ARA&A, 38, 379
- Volonteri, M., P., Saracco, P., Chincarini, G., & Bolzonella, M. 2000, A&A, 362, 487
- Vreeswijk, P. M., Rol, E., Hjorth, J., et al. 1999, GRB Circular Network, 496
- Vreeswijk, P. M., Fruchter, A., Ferguson, H., & Kouveliotou, C. 2000, GRB Circular Network, 751, 1
- Vreeswijk, P. M., Fruchter, A., Kaper, L., et al. 2001, ApJ, 546, 67
- Williams, R. E. et al. 1996, AJ, 112, 1335
- Woosley, S. E. 1993, ApJ, 405, 273

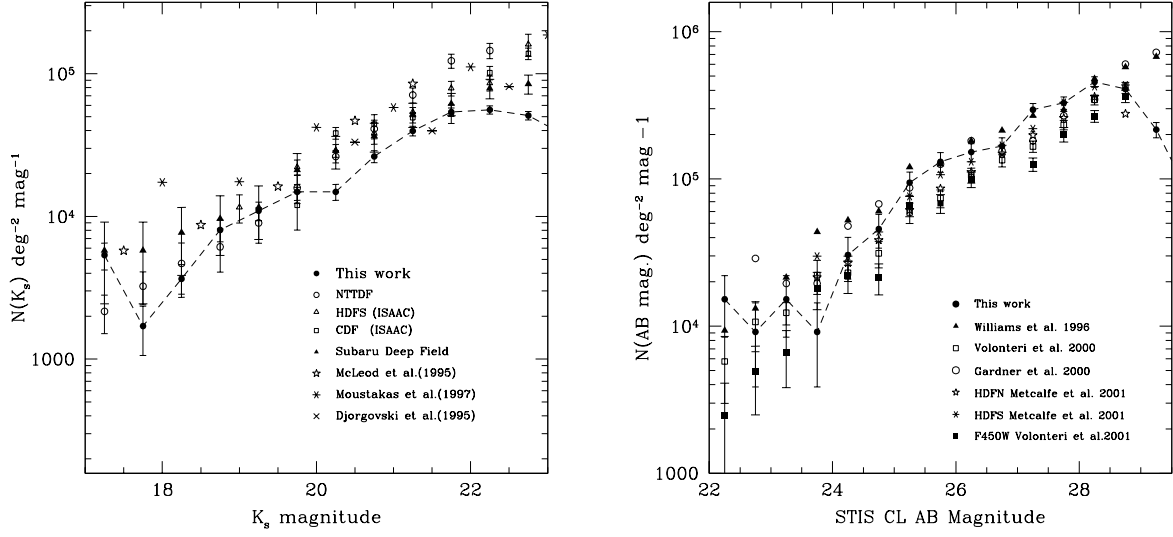


Fig. 1.— Near-IR number counts in the ISAAC images (left panel) and optical number counts in *HST*/STIS images (right panel) for GRB fields and determinations from the literature.

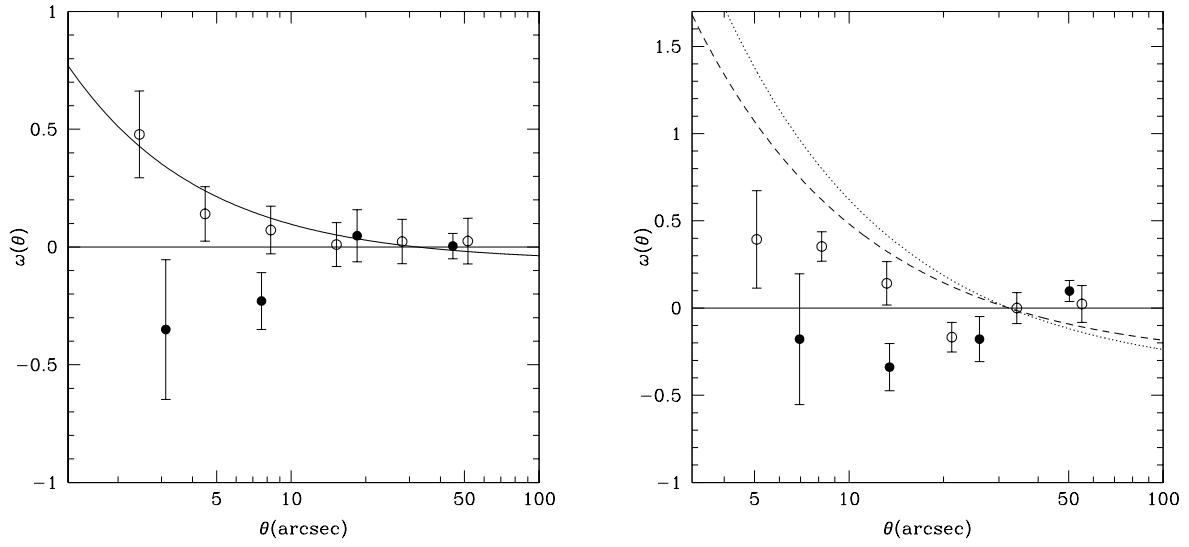


Fig. 2.— Two point cross-correlation functions GRB-tracer galaxies (filled circles) and auto-correlation functions of tracers galaxies (open circles). Left panel: $K_s < 21.5$. Solid line is the best power law fit to auto-correlation for tracer galaxies with $K_s < 21.5$. Right panel: $K_s < 19$. The dotted line correspond to $K < 19$ radio galaxy-galaxy correlation function taken from Best (2000). The dashed line corresponds to USS-galaxy correlation function for tracers with $18 < K < 19$ taken from Bornancini et al. (2004)

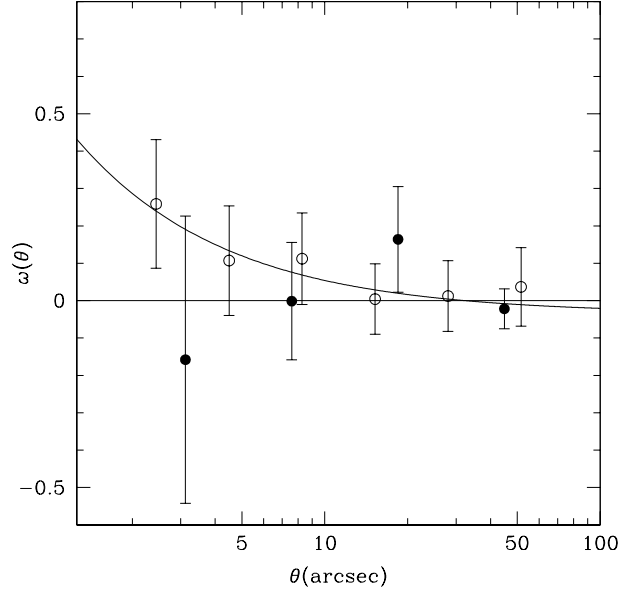


Fig. 3.— Same as previous figure but tracer galaxies restricted to $19.5 < K_s < 21.5$

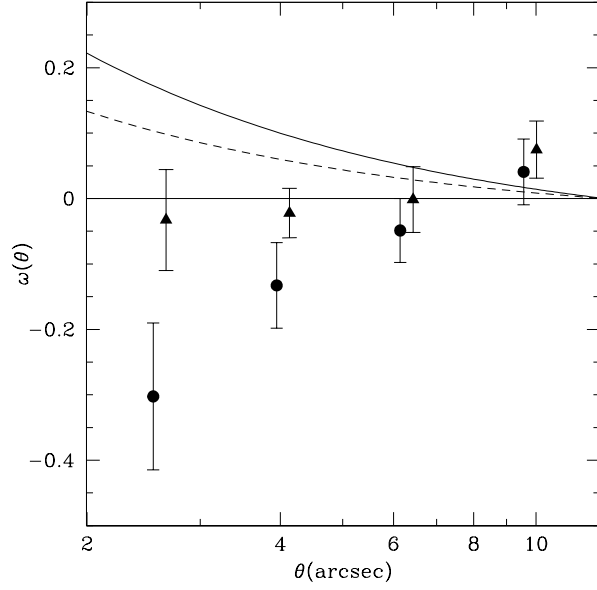


Fig. 4.— GRB-tracer galaxies ($CL < 28$) cross-correlation function in the *HST*/STIS images and for all GRB hosts quoted in Table 2 (filled triangles), the filled circles correspond to GRB hosts in the redshift range $0.7 < z < 2$. Solid line is the best power law fit to auto-correlation function for tracer galaxies with $CL < 28$. Dotted line corresponds to auto-correlation function for GRB hosts in the redshift range $0.7 < z < 2$

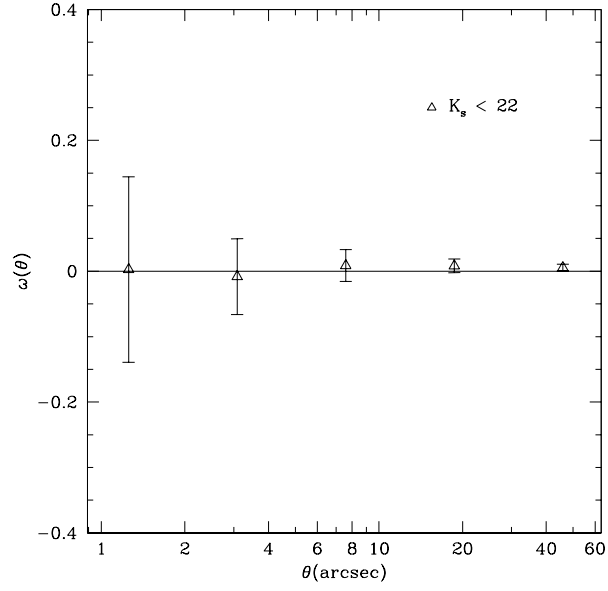


Fig. 5.— Star auto-correlation function test

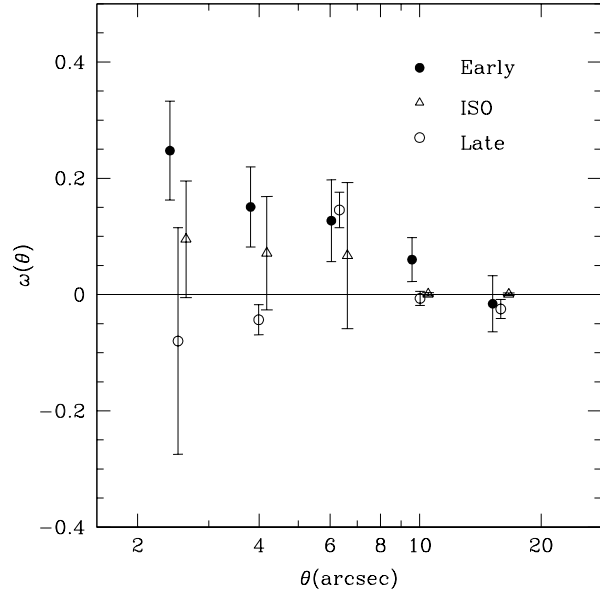


Fig. 6.— Cross-correlation functions between particular galaxy targets and tracers galaxies with $F606 < 27$

Table 1. GRB hosts ISAAC observations

Name	R.A. (J2000)	Dec. (J2000)	z	Reference	K_s^1	Limiting Magnitude (1.5σ)
GRB 981226	23 ^h 29 ^m 37 ^s .2	−23° 55′ 54″	$\sim 1^\dagger$	1	21.10±0.1	24.4
GRB 990506	11 ^h 54 ^m 50 ^s .1	−26° 40′ 35″	1.30	2	21.45±0.2	24.4
GRB 990510	13 ^h 38 ^m 07 ^s .1	−80° 29′ 48″	1.62	3	≥ 22.5	22.5
GRB 000210	01 ^h 59 ^m 15 ^s .5	−40° 39′ 33″	0.85	4	20.95±0.2	23.4
GRB 000418	12 ^h 25 ^m 19 ^s .3	+20° 06′ 11″	1.12	2	21.30±0.2	24.5
GRB 001011	18 ^h 23 ^m 04 ^s .6	−50° 54′ 16″	$\sim 1^\dagger$	1	21.45±0.2	23.4

References. — (1) Le Floc’h et al. 2003 ; (2) Bloom et al. 2003 ; (3) Vreeswijk et al. 2001 ; (4) Piro et al. 2002 .

Table 2. STIS 50CCD GRB hosts sample characteristics

Name	Ref.	R.A. (J2000)	Dec. (J2000)	z	Ref.	CL	Ref.	exp. time (seconds)	Limiting Mag. (2σ)
GRB 970228	1	05 ^h 01 ^m 46 ^s .7	+11° 46′ 53″	0.695	20	25.8 ± 0.25	1	2300	29.0
GRB 970508	2	06 ^h 53 ^m 49 ^s .5	+79° 16′ 20″	0.835	21	25.25 ± 0.20	2	11688	30.3
GRB 971214	3	11 ^h 56 ^m 26 ^s .4	+65° 12′ 01″	3.42	22	25.68 ± 0.05	(*) ^a	11874	29.7
GRB 980326	4	08 ^h 36 ^m 34 ^s .3	+79° 16′ 20″	1?	23	29.25 ± 0.25	4	7200	27.5
GRB 980329	5	07 ^h 02 ^m 38 ^s .0	+38° 50′ 44″	< 4	24	28.6±0.3	5	8072	28.2
GRB 980519	6	23 ^h 22 ^m 21 ^s .5	+77° 15′ 43″	> 1.5	25	27.0 ± 0.2	37	8983	29.6
GRB 980613	7	10 ^h 17 ^m 57 ^s .6	+71° 27′ 26″	1.096	26	26.3 ± 0.1	7	5851	28.7
GRB 980703	8	23 ^h 59 ^m 06 ^s .7	+08° 35′ 07″	0.966	27	23.00 ± 0.10	8	5178	29.2
GRB 981226	9	23 ^h 29 ^m 37 ^s .2	−23° 55′ 54″	$\sim 1^\dagger$	28	25.04 ± 0.07	9	8265	28.2
GRB 990123	10	15 ^h 25 ^m 30 ^s .3	+44° 45′ 59″	1.6	29	25.45 ± 0.15	10	7800	29.7
GRB 990308	11	12 ^h 23 ^m 11 ^s .4	+06° 44′ 05″	> 1.2?	30	29.7 ± 0.4	37	7842	29.0
GRB 990506	12	11 ^h 54 ^m 50 ^s .1	−26° 40′ 35″	1.3	31	24.5 ± 0.1	(*) ^b	7914	29.2
GRB 990510	13	13 ^h 38 ^m 07 ^s .3	−80° 29′ 49″	1.619	32	28 ± 0.3	13	5840	29.2
GRB 990705	14	05 ^h 09 ^m 54 ^s .5	−72° 07′ 53″	0.843	33	22.45 ± 0.10	33	8851	29.6
GRB 990712	15	22 ^h 31 ^m 53 ^s .0	−73° 24′ 28″	0.430	32	~ 23	15	4080	29.5
GRB 991208	16	16 ^h 33 ^m 53 ^s .5	+46° 27′ 22″	0.706	34	24.6 ± 0.15	16	5120	30.0
GRB 991216	17	05 ^h 09 ^m 31 ^s .3	+11° 17′ 07″	1.02	35	26.63 ± 0.12	(*) ^c	4744	28.9
GRB 000418	18	12 ^h 25 ^m 19 ^s .3	+20° 06′ 11″	1.12	31	24.30±0.03	(*) ^a	5120	29.5
GRB 000301	19	16 ^h 20 ^m 18 ^s .6	+29° 26′ 36″	2.04	36	27.55 ± 0.04	(*) ^a	73911	31.7

References. — (1) Fruchter et al. 1999a ; (2) Fruchter & Pian 1998 ; (3) Odewahn et al. 1998 ; (4) Fruchter, Vreeswijk, & Nugent 2001 ; (5) Holland 2000a ; (6) Holland et al. 2000a ; (7) Holland 2000b ; (8) Holland et al. 2001 ; (9) Holland 2000c ; (10) Fruchter et al. 1999 ; (11) Holland 2000d ; (12) Hjorth 2000 ; (13) Fruchter, Hook, & Pian 2000 ; (14) Holland et al. 2000b ; (15) Fruchter et al. 2000 ; (16) Fruchter, Vreeswijk, Sokolov, & Castro-Tirado 2000 ; (17) Vreeswijk, Fruchter, Ferguson, & Kouveliotou 2000 ; (18) Fruchter & Metzger 2001 ; (19) Fruchter & Vreeswijk 2001 ; (20) Bloom, Djorgovski & Kulkarni 2001 ; (21) Bloom et al. 1998 ; (22) Kulkarni et al. 1998 ; (23) Bloom et al. 1999 ; (24) Lamb, Castander, & Reichart 1999 ; (25) Jaunsen et al. 2001 ; (26) Djorgovski, Bloom, & Kulkarni 2003 ; (27) Djorgovski et al. 1998 ; (28) Le Floc’h et al. 2003 ; (29) Hjorth et al. 1999 ; (30) Schaefer et al. 1999 ; (31) Bloom et al. 2003 ; (32) Vreeswijk et al. 2001 ; (33) Le Floc’h et al. 2002 ; (34) Castro-Tirado et al. 2001 ; (35) Vreeswijk et al. 1999 ; (36) Jensen et al. 2001 ; (37) Jaunsen et al. 2003 ;

(*) This Work.

^{a,b,c} In a aperture of radius 1′0, 2′5, 0′′5.

Note. — † : Derived from their K magnitude and $R - K$ color.